Gas flow through a micro-orifice due to small pressure difference

Sarantis PANTAZIS*, Dimitris VALOUGEORGIS

* Corresponding author: Tel.: ++30 24210 74336; Fax: ++30 24210 74085; Email: spantazis@mie.uth.gr
Department of Mechanical Engineering, University of Thessaly, Volos, GR

Abstract Rarefied gas flow through a micro-orifice connecting two reservoirs at small pressure differences is considered in the whole range of rarefaction by the linearized BGK kinetic model equation. The problem is computationally challenging due to the five dimensional nature of the distribution function and techniques such as parallelization and numerical schemes of low memory requirements have been applied. Results include the distributions of density, velocity, temperature, as well as flow rates. The independence of flow rate in terms of the wall surface accommodation properties is confirmed.

Keywords: Linearized kinetic theory, rarefied gas dynamics, Knudsen number, orifice

1. Introduction

The problem of flow through an orifice, i.e. a cylindrical tube of zero length, is quite interesting for several applications. Orifices are frequently encountered in microfluidic networks (Aktas et al., 2001), while they also possess the property of producing results independent of the wall accommodation properties (Liepmann, 1961; Sharipov and Seleznev, 1998). Thus, the apparatus can be realized experimentally and used as a test for numerical methods and intermolecular potential models.

Long channels, whose length is more than 100 times larger than its radius, have been studied both numerically and experimentally by several researchers (Cercignani, 1979; Sharipov and Seleznev, 1994; Naris et al., 2005) and for various geometries (Naris and Valougeorgis, 2008; Breyannis et al., 2008; Graur and Sharipov, 2007; Pantazis et al., 2010; Varoutis et al., 2009a). However, short channels are much more difficult to consider. This is attributed to the five- or six-dimensional nature of the distribution function and the fact that the complete flow field, along with a part of the upstream/downstream vessels, must be included in the simulations.

Since the usual Navier-Stokes formulation is not applicable in the microscale, the most wide-spread approaches for dealing with rarefied gases are based on Monte Carlo methods, such as the DSMC (Bird, 1994). For large pressure differences and in the whole range of the Knudsen number, DSMC is very often used due to its simplicity and the ability to correctly describe highly non-equilibrium flows with good computational efficiency. For this reason, it has already been applied not only in the case of orifice flow (Sharipov, 2004; Alexeenko et al., 2001; Taniguchi et al., 1996) but also for channels of non-zero length (Varoutis et al., 2009b; Sazhin, 2009).

However, in the low pressure difference regime, this method converges very slowly due to the increased statistical noise and the computational time becomes prohibitive. Remedies for this kind of difficulties exist (Hadjiconstantinou and Baker, 2008) but they are not so easily implemented. In this regime, the numerical solution of linearized kinetic model equations is traditionally applied. The linearization leads to a system of equations with a well established mathematical background, providing very accurate results for slow flows. It has also been found in other configurations (Pantazis and Valougeorgis, 2010) that linearized results may also be valid in a wider range of conditions than expected by the strict mathematical limits.

The kinetic model equations have been discretized in the 2D physical and 3D molecular velocity space, employing the

Discrete Velocity Method (DVM). The numerical code is parallelized in the molecular velocity space and memory requirements are drastically reduced by adjusting the storage scheme of the distribution function according to the numerical marching algorithm. A non-uniform grid is applied in physical space, in order to capture large gradients of the macroscopic quantities. Results are provided for the macroscopic quantities, such as number density, temperature and velocity but also for flow rates. Furthermore, a comparison with DSMC data is given.

2. Formulation

Consider two containers maintained at slightly different pressures ($P_0 + \Delta P$ upstream, P_0 downstream), connected by an orifice of radius R through which the rarefied gas flows, as seen in Fig. 1. Both containers are kept at a constant temperature T_0. The steady state BGK kinetic model equation may be applied here

$$\xi_r \frac{\partial f}{\partial \hat{r}} - \frac{\xi_\vartheta}{\hat{r}} \frac{\partial f}{\partial \theta} + \xi_x \frac{\partial f}{\partial \hat{x}} = \nu \left(f^M - f \right) \quad (1)$$

where $\hat{r}$ is the radial coordinate ($0 \le \hat{r} \le R$ in the orifice), $\boldsymbol{\xi} = \left(\xi_r, \xi_\vartheta, \xi_x \right)$ is the molecular velocity vector, θ is the angle of the molecular velocity in the $\hat{r} - \vartheta$ plane ($0 \le \theta \le 2\pi$), f is the unknown distribution function, ν is the collision frequency and f^M is the Maxwellian distribution of particles.

Due to the small relative size of the pressure difference $\left(\Delta P / P_0 \ll 1 \right)$, the distribution function may be linearized as

$$f = f_0 \left(1 + h \frac{\Delta P}{P_0} \right) \quad (2)$$

where f_0 is a Maxwellian distribution at the reference conditions. Our purpose is to calculate the perturbation of the distribution function $h = h\left(\hat{r}, \hat{x}, \xi_r, \xi_\vartheta, \xi_x \right)$.

For reasons of convenience and generality, all quantities are expressed in dimensionless form according to the following expressions:

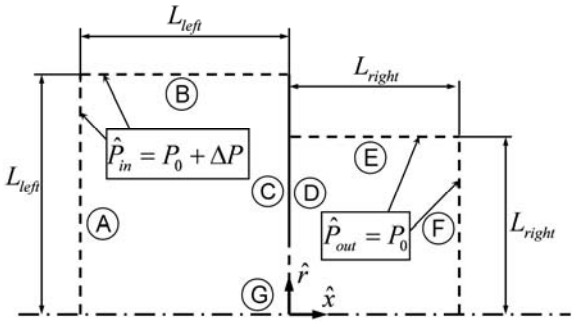

Figure 1: Geometry and boundary surface definition

$$r = \frac{\hat{r}}{R}, x = \frac{\hat{x}}{R}, \mathbf{c} = \frac{\boldsymbol{\xi}}{\upsilon_0}, \upsilon_0 = \sqrt{2 \frac{k_B}{m} T_0} \quad (3)$$

with υ_0 being the most probable molecular velocity and k_B is the Boltzmann constant. The macroscopic quantities $\psi(r,x)$ may be found by calculating their perturbation $\phi(r,x)$ from the reference quantities ψ_0, according to the expression

$$\phi(r,x) = \frac{\psi(r,x) - \psi_0}{\psi_0} \frac{P_0}{\Delta P}. \quad (4)$$

For practical applications, we are interested in the number density

$$\phi = \rho, \ \psi = n, \ \psi_0 = n_0 \quad (5)$$

the temperature

$$\phi = \tau, \ \psi = T, \ \psi_0 = T_0 \quad (6)$$

the pressure

$$\phi = P, \ \psi = \hat{P}, \ \psi_0 = P_0 \quad (7)$$

and the bulk velocity vector

$$\phi = \boldsymbol{u}, \ \psi = \hat{\boldsymbol{u}}, \ \psi_0 = 0 \quad (8)$$

The right container conditions are taken as reference quantities. The degree of rarefaction is described by the rarefaction parameter δ, defined here as

$$\delta = \frac{R P_0}{\mu_0 \upsilon_0} \sim \frac{1}{Kn} \quad (9)$$

with μ_0 being the gas viscosity at reference temperature T_0. This parameter is inversely proportional to the Knudsen number.

As a final step, the molecular velocity vector $\mathbf{c} = \left(c_r, c_\vartheta, c_x \right)$ is transformed to cylindrical coordinates $\mathbf{c} = \left(c_p, \theta, c_x \right)$. The components of the molecular velocity are shown in Fig. 2 and are more appropriate for

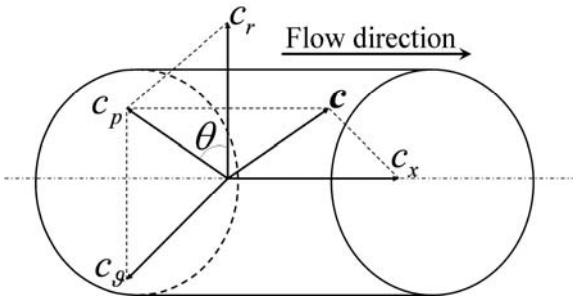

Figure 2: Molecular velocity coordinate system

the current problem. Thus, the final equation is

$$c_p\cos\theta\frac{\partial h}{\partial r}-\frac{c_p\sin\theta}{r}\frac{\partial h}{\partial\theta}+c_x\frac{\partial h}{\partial x}+\delta h= \\ =\delta\left[\rho+\tau\left(c^2-\frac{3}{2}\right)+2\boldsymbol{c}\cdot\boldsymbol{u}\right] \quad (10)$$

The macroscopic quantity perturbations are expressed in terms of the perturbation h by

$$\rho=\frac{1}{\pi^{3/2}}\int_{-\infty}^{\infty}\int_0^{2\pi}\int_0^{\infty}hc_pe^{-c^2}dc_pd\theta dc_x \quad (11)$$

$$u_r=\frac{1}{\pi^{3/2}}\int_{-\infty}^{\infty}\int_0^{2\pi}\int_0^{\infty}h\left(c_p\cos\theta\right)c_pe^{-c^2}dc_pd\theta dc_x \quad (12)$$

$$u_x=\frac{1}{\pi^{3/2}}\int_{-\infty}^{\infty}\int_0^{2\pi}\int_0^{\infty}hc_xc_pe^{-c^2}dc_pd\theta dc_x \quad (13)$$

$$\tau=\frac{1}{\pi^{3/2}}\int_{-\infty}^{\infty}\int_0^{2\pi}\int_0^{\infty}h\left(\frac{2}{3}c^2-1\right)c_pe^{-c^2}dc_pd\theta dc_x \quad (14)$$

The formulation is completed by providing the boundary conditions. Molecules entering from the free surfaces (A),(B),(E),(F) (as shown in Fig. 1) conform to a Maxwellian distribution according to the conditions of the corresponding boundary. At the boundary surfaces (A),(B),we have $n=n_0+\Delta n$, $T=T_0$ and $\hat{\boldsymbol{u}}=0$ and therefore the perturbation from the equilibrium distribution is

$$h_{A,B}^{+}=\rho_{in}=1 \quad (15)$$

Similarly, it is found that in the downstream free surfaces (E),(F) the perturbation of the incoming distribution is

$$h_{E,F}^{+}=0 \quad (16)$$

For the walls (C),(D), diffuse-specular boundary conditions are imposed

$$h_{C,D}^{+}=\alpha\rho_{C,D}+(1-\alpha)h_{C,D}^{-} \quad (17)$$

where $h_{C,D}^{-}$ is the appropriate impinging component in the specular direction. The constants $\rho_{C,D}$ are found using the impermeability condition $\left(u_{normal}=0\right)$ and the macroscopic velocity integrals (12) and (13). Finally, at the surface (G), coinciding with the axis of symmetry $\left(r=0\right)$, molecules are reflected specularly, i.e.

$$h_G^{+}\left(c_p,\theta,c_x\right)=h_G^{-}\left(c_p,\pi-\theta,c_x\right) \quad (18)$$

where $\theta\in\left[0,\pi/2\right]$.

The most important quantity for the practical applications is the mass flow rate through the channel, which is non-dimensionalized by the analytical solution for flow through an orifice under free molecular conditions $\left(\delta=0\right)$. This solution can be easily extracted by the method of characteristics and yields

$$\dot{M}_{FM}=R^2\sqrt{\pi}\frac{\Delta P}{\upsilon_0} \quad (19)$$

The dimensionless flow rate W is equal to

$$W=\frac{\dot{M}}{\dot{M}_{FM}}=4\sqrt{\pi}G \quad (20)$$

where

$$G\big|_x=\int_0^1u_x(r,x)rdr \quad (21)$$

is the reduced flow rate.

3. Numerical scheme

The numerical scheme is based on the Discrete Velocity Method for the treatment of the molecular velocity space. The continuum spectrum of the molecular velocity magnitudes c_p and c_x is discretized by the Legendre polynomial roots mapped in $[0,c_{p,max}]$ and $[0,c_{x,max}]$ respectively, while the molecular velocity angles are uniformly distributed in $[0,\pi]$ due to the axisymmetrical properties of the flow. The solution is obtained by an iterative procedure, where the main unknown is the distribution function h. At first, an assumption is made for the macroscopic quantity perturbations. This estimation is used in combination with the governing equation (10) to calculate the value of the distribution function h. The distribution function is

further used to generate new values for the bulk quantities via the corresponding moments (11)-(14). These quantities are re-used in the governing equation to obtain new estimates for h and this procedure is repeated until a proper convergence criterion, imposed on the bulk quantities, is satisfied. A second order finite volume scheme has been applied here, derived in the same way as in (Pantazis and Valougeorgis, 2010) by integrating the governing equation in r,θ,x in an arbitrary discretization interval, acting in both parts of (10) with the operator

$$A=\int_{x_k-\frac{\Delta x_k}{2}}^{x_k+\frac{\Delta x_k}{2}}\int_{\theta_j-\frac{\Delta\theta_j}{2}}^{\theta_j+\frac{\Delta\theta_j}{2}}\int_{r_i-\frac{\Delta r_i}{2}}^{r_i+\frac{\Delta r_i}{2}}(\cdot)drd\theta dx \qquad (22)$$

Then, all integrations can either be carried out analytically or substituted by the trapezoidal rule, causing the second-order error. We also substitute $\cos\theta_j=\left(\cos\theta_{j+1/2}+\cos\theta_{j-1/2}\right)/2$ and $\sin\theta_j=\left(\sin\theta_{j+1/2}+\sin\theta_{j-1/2}\right)/2$ since the expression $\cos\left[\left(\theta_{j+1/2}-\theta_{j-1/2}\right)/2\right]\cong 1$ is a very good approximation for small $\Delta\theta_j$. The final discretized equation does not appear here due to its size, but is given in (Pantazis, 2011).This expression is applied for any interval, regardless of the grid distances Δr_i, Δx_k and the angle discretization $\Delta\theta_j$ and is also usable as $r\to 0$ after the application of the l'Hospital rule on the indeterminate fractions.

The computational effort can be distributed in several processors by noticing that the distribution functions of different velocity magnitudes can be calculated independently from one another. As a result, the code can be easily parallelized in the molecular velocity space. Each processor solves the kinetic equation for a group of velocities and information on macroscopic quantities and impermeability constants is exchanged between the processors at the end of each iteration. In this manner, the transmition of the distribution is circumvented, greatly reducing the cost of parallel communication.

Table 1: Computational parameters

Minimum $\Delta x_0=\Delta r_0$	1.6×10^{-3}
Grid parameter η	0.01
Discrete angles in $[0,\pi]$	100
Discrete magnitudes c_p, c_x	16×16
Max. magnitude $c_{p,\max}$, $c_{x,\max}$	5
Convergence criterion per node	10^{-7}

Memory handling techniques have also been used to reduce storage requirements due to the five dimensional nature of the distribution function for this problem (Pantazis, 2011). Due to the velocity magnitude independency, a temporary array can be allocated and overwritten after treating each magnitude. Also, the dimensionality of this array is reduced even more by storing the distribution only in the parts of the domain required by the marching scheme of the discretized governing equation. For example, for motion towards the positive x direction, the distribution is stored only at positions x and $x-\Delta x$. These techniques permit having a two-dimensional array for the distribution function and greatly reduce memory limitations. In this manner, large size domains can be considered, since the size of the distribution array is only determined by the height of the entrance/exit regions and the number of the molecular velocity angles.

The discretization parameters used are displayed in Table 1. The computational grid is non-uniform, with particular emphasis on the accuracy near the corners. The grid distances varied in the range $x>0$ according to $\Delta x_i=(1+\eta)\Delta x_{i-1}$ and similarly for other directions in both r,x as we move away from the corner. For the results shown here, there are 200 nodes in the first unit length around the corners and the total number in the whole domain is up to 10^6. The average residual per computational node has been chosen as the convergence criterion.

It is well known (Hasegawa and Sone, 1990) that the upstream/downstream regions must be quite large, since the mass conservation law indicates that the

macroscopic quantities converge to the uniform container values at a very high distance from the tube. Therefore, container regions of size $L_{left} = L_{right}$ ranging from $15R$ to $50R$ were used, after verifying that results do not change for larger values by parameterization runs.

The fulfillment of the mass conservation principle

$$\frac{1}{r}\frac{\partial(ru_r)}{\partial r} + \frac{\partial u_x}{\partial x} = 0 \qquad (23)$$

was examined by calculating the left hand side of (21) in the whole field, where it was shown that all values are very close to zero. Furthermore, the flow rate (18) was calculated for all cases in several positions and it was found to be constant in at least three significant figures.

4. Results

Numerical results include quantities of practical interest, such as the flow rate, streamlines and contours for the most important macroscopic quantities. The dimensionless flow rate W obtained by the current linearized formulation is shown in the third column of Table 2 (denoted as "Lin. DVM") for a wide range of the rarefaction parameter. The flow rate increases monotonically and very steeply in the region of high δ. Furthermore, the same Table includes directly comparable flow rate values given by the non-linear BGK model and the Discrete Velocity Method for $P_{out} = 0.9$ (Pantazis, 2011), as well as the corresponding DSMC results (Sharipov, 2004) for the same pressure ratio. The flow rate values for the non-linear formulations have been properly adjusted by $W_{Lin} = W_{NL/DSMC} / (1 - P_{out} / P_{in})$ to correspond to each other. It is seen that a very good agreement is found with the non-linear BGK model for all values of δ tested here, with a maximum difference of 2.3%. This is another confirmation of the validity of the current results. Furthermore, it is an indication that the linearized formulation is valid for a range of pressure differences larger than it was initially expected ($\Delta P / P_0 = 0.1$ while the linearization condition is that $\Delta P / P_0 \ll 1$). The DSMC method produces significantly smaller flow rates for large δ values. A part of this deviation may be attributed to the use of the BGK model, but from previous studies discussed in (Sharipov and Seleznev, 1998) this is not expected to cause such large differences for small pressure differences. Since the statistical noise is very strong for this pressure ratio and especially for the large δ case, we may infer that the discrepancy is probably due to numerical and computational limitations of DSMC. Furthermore, the significantly smaller size of upstream and downstream regions in (Sharipov, 2004) ($L_{left} = L_{right} = 8R$) may have also influenced the results. In any case, since the orifice is a highly non-linear case, it can be assumed that a lower deviation is to be expected for longer channels.

Table 2: Flow rate W for diffuse reflection

		Lin. DVM	NL DVM	DSMC
δ	0	0.999	1.00	-
	0.01	1.00	1.00	-
	0.1	1.04	1.05	1.03
	0.5	1.19	1.21	-
	1	1.37	1.40	1.30
	2	1.72	1.76	-
	5	2.77	2.80	-
	10	4.35	4.32	4.02

The flow rate increases monotonically along with the rarefaction parameter. The Knudsen minimum is not observed at all for the orifice case, as confirmed by previous studies. This seems reasonable, if we consider that the minimum occurs because of the molecular beaming phenomenon, which can not appear for short tubes or orifices.

Table 3: Flow rate W for incomplete accommodation

α		0.5	0.8
δ	0	1.00	0.999
	0.1	1.04	1.04
	1	1.37	1.37
	10	4.35	4.35

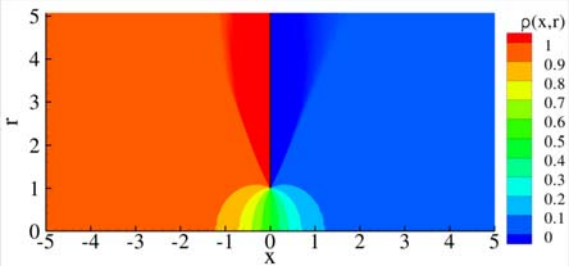

Figure 3: Perturbation of number density for $\delta = 1$.

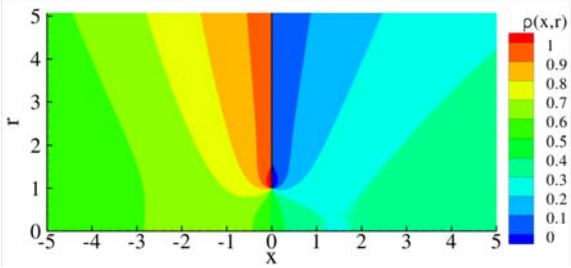

Figure 8: Perturbation of number density for $\delta = 10$.

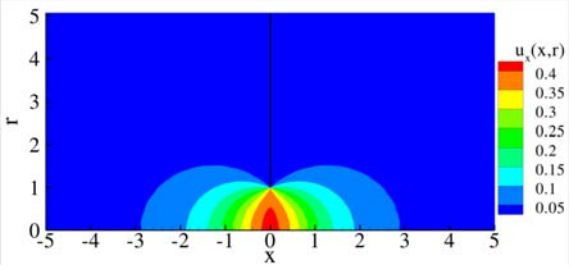

Figure 4: Perturbation of axial velocity for $\delta = 1$.

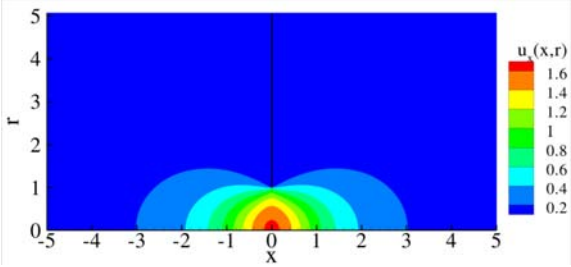

Figure 9: Perturbation of axial velocity for $\delta = 10$.

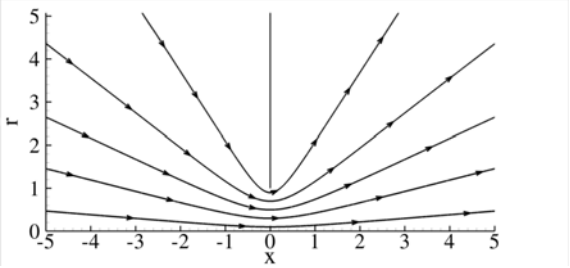

Figure 5: Streamlines for $\delta = 1$.

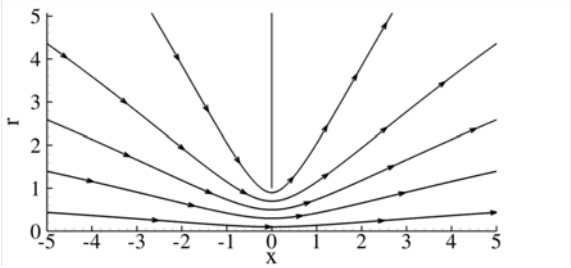

Figure 10: Streamlines for $\delta = 10$.

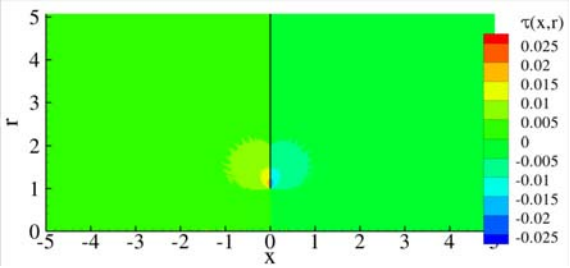

Figure 6: Perturbation of temperature for $\delta = 1$.

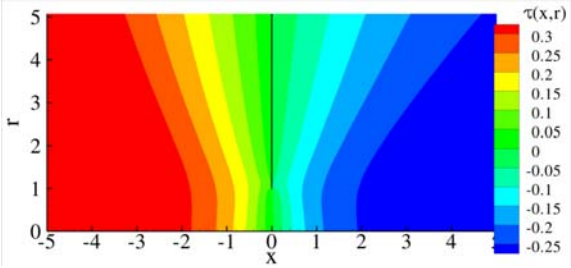

Figure 11: Perturbation of temperature for $\delta = 10$.

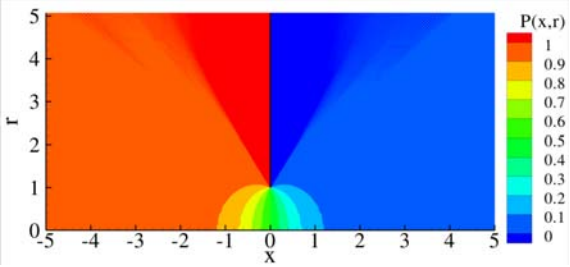

Figure 7: Perturbation of pressure for $\delta = 1$.

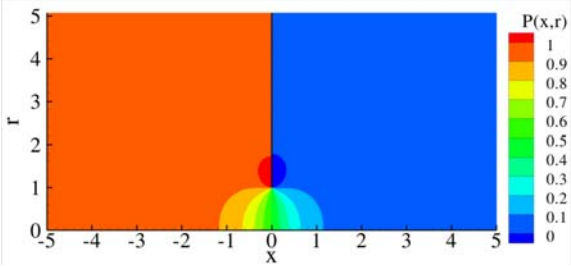

Figure 12: Perturbation of pressure for $\delta = 10$.

Indicative results for incomplete accommodation are also presented in Table 3. It is seen that at all cases considered here, the flow rate remains nearly constant and independent of the accommodation coefficient. This is a very significant property of this flow, making it an ideal experimental setup for comparison with experimental data in order to study the behaviour and quality of the models, the numerical scheme, or even the experimental apparatus itself.

Macroscopic variable perturbation fields are also presented in Figs. 4-8 for $\delta = 1$ and in Figs. 9-13 for $\delta = 10$. In every case, the fields display symmetrical properties in the whole range of rarefaction due to the small pressure difference, resulting to a very low Reynolds number. The density field varies between the equilibrium values of the two containers, while a much larger area of the containers is affected at large value of δ. The axial velocity also increases as δ is increased. Streamlines are practically identical for the two cases. The temperature perturbation is nearly zero for $\delta = 1$ but obtains non-negligible values for $\delta = 10$. Its form is justified if we consider that the pressure perturbation is given by $p = \rho + \tau$. Thus, the temperature isolines have a similar form to the corresponding ones for density and as a result, the pressure perturbation obtains the well known form, given in Figs. 8 and 13. In future work, the BGK model may be replaced by the ES or S kinetic models to examine for possible effects of the temperature perturbation.

Acknowledgements

This work has been supported by the European Community under the contract of Association EURATOM / Hellenic Republic. The views and opinions expressed herein do not necessarily reflect those of the European Commission.

References

Aktas, O., Aluru, N.R., Ravaioli, U., 2001. Application of a parallel DSMC technique to predict flow characteristics in microfluidic filters. Journal of Microelectromechanical Systems 10, 538–549.

Alexeenko, A.A., Levin, D.A., Gimelshein, S.F., Ivanov, M.S., Ketsdever, A.D., 2001. Numerical and Experimental Study of Orifice Flow in the Transitional Regime. 35th Thermophysics Conference, AIAA Paper 2001–3072.

Bird, G.A., 1994. Molecular Gas Dynamics and the Direct Simulation of Gas Flows. Oxford University Press, Oxford.

Breyannis, G., Varoutis, S., Valougeorgis, D., 2008. Rarefied gas flow in concentric annular tube: Estimation of the Poiseuille number and the exact hydraulic diameter. European Journal of Mechanics - B/Fluids 27, 609–622.

Cercignani. C., 1979. Rarefied gas flow through long slots. Journal of Applied Mathematics and Physics (ZAMP) 30, 943–951.

Graur, I., Sharipov, F., 2007. Gas flow through an elliptical tube over the whole range of the gas rarefaction. European Journal of Mechanics - B/Fluids 27, 335–345.

Hadjiconstantinou, N.G., Baker, L.L., 2008. Variance-reduced monte carlo solutions of the Boltzmann equation for low-speed gas flows: A discontinuous Galerkin formulation. International Journal for Numerical Methods in Fluids 58, 381–402.

Hasegawa, M., Sone, Y., 1990. Rarefied gas flow through a slit. Physics of Fluids A 3, 466–477.

Liepmann, H.W., 1961. Gas kinetic and gas dynamics of orifice flow. Journal of Fluid Mechanics 10, 65–79.

Naris, S., Valougeorgis, D., Sharipov, F., Kalempa, D., 2005. Flow of gaseous mixtures through rectangular microchannels driven by pressure, temperature, and concentration gradients. Physics of Fluids 17, 100607.1–100607.12.

Naris, S., Valougeorgis, D., 2008, Rarefied gas flow in a triangular duct based on a boundary fitted lattice. European Journal of Mechanics - B/Fluids 27, 810–822.

Pantazis, S., Varoutis, S., Hauer, V., Day, C., Valougeorgis, D., 2010. Gas-surface

scattering effect on vacuum gas flows through rectangular channels. 11th European Vacuum Conference.

Pantazis, S., Valougeorgis, D., 2010. Heat transfer through rarefied gases between coaxial cylindrical surfaces with arbitrary temperature difference. European Journal of Mechanics - B/Fluids 29, 494–509.

Pantazis, S., 2011. Ph.D. dissertation, Department of Mechanical Engineering, University of Thessaly.

Sazhin, O., 2009. Gas molecule-molecule interaction and the gas-surface scattering effect on the rarefied gas flow through a slit into a vacuum. Journal of Experimental and Theoretical Physics 108, 874–879.

Sharipov, F., Seleznev, V., 1994, Rarefied gas flow through a long tube at any pressure ratio. Journal of Vacuum Science and Technology A 12, 2933–2935.

Sharipov, F., Seleznev, V., 1998. Data on internal rarefied gas flows. J. Phys. Chem. Ref. Data 27, 657–706.

Sharipov, F., 2004. Numerical simulation of rarefied gas flow through a thin orifice. Journal of Fluid Mechanics 518, 35–60.

Taniguchi, H., Ota, M., Aritomi, M., 1996. Effects of surface boundary conditions on transmition probabilities through circular tubes. Vacuum 47, 787–790.

Varoutis, S., Naris, S., Hauer, V., Day, C., Valougeorgis, D., 2009a. Computational and experimental study of gas flows through long channels of various cross sections in the whole range of the Knudsen number. J. Vac. Sci. Technol. A 27, 89–100.

Varoutis, S., Valougeorgis, D., Sharipov, F., 2009b. Simulation of gas flow through tubes of finite length over the whole range of rarefaction for various pressure drop ratios. J. Vac. Sci. Technol. A 27, 1377–1391.